

Data Product Overview

The photometric modeling data products are Radiance Factor (RADF - a unit equivalent to the quantity I/F) functions called photometric models that describe the scattering behavior of the asteroid surface as a function of viewing geometry, illumination geometry, and wavelength. The photometric models are derived for each channel (wavelength) of the OVIRS spectral data. These models serve the practical purpose of photometrically correcting the OVIRS data such that the spectra can be compared with each other even when illumination or viewing angles differ.

Overview

What is the data type (image, spectrum, data table, map format etc.)?

FITS File Image extensions that contain the photometric model parameters for each wavelength as 2-D arrays.

What does it measure at what scale?

The model doesn't measure anything, it uses the spectral data (spectral measurements at a wide range of observing viewing angles (incidence, emission, and phase)) to predict the radiance from the surface at un-measured viewing and illumination geometries. The model is relevant to the spatial scale represented by the input data. For OVIRS, this means 6-19 meter diameter round spots over 80% of the surface of Bennu.

The model uses I/F , measured at a wide range of observing viewing angles (incidence, emission, and phase), to develop a globally averaged prediction of the reflectance of the surface as a function of viewing angle.

The "best fit" model - based on visual inspection as a function of incidence, emission, and phase angle - will be selected from among three possible functional forms:

Modified Lommel-Seeliger

ROLO

Modified Minnaert

Each wavelength of the OVIRS data will have its own model.

What MRD does this data product contribute to satisfying?

Spectral Analysis:

MRD-118

MRD-140

MRD-143

MRD-147

MRD-154

MRD-159

Regolith Development:

MRD-542

What observations are required to provide the input data needed to make the data product?

OVIRS spectra from Detailed Survey are required to make this data product: specifically, observations from the following Detailed Survey stations:

- 12:30 station (phase angle = 5 degrees)
- 10:00am station (phase angle = 30 degrees)
- 3:00pm station (phase angle = 45 degrees)
- 6pm (or 6am) station (phase angle = 90 degrees)

For each station, we require observations that cover as wide a range of incidence and emission angles as possible. Since Bennu is roughly round, it is expected that this means observations from the north to the south across the disk (or vice versa). To some extent, the time-of-day of the station (or the phase angle) determines the range of incidence and emission angles available. Our main goal is to make sure we sample the full range available at each station for the purposes of constraining the scattering behavior of the surface.

Requirements Levied on the Observations by this Data Product

- It is important to note that data from a wide range of incidence, emission and phase angles are critical to the development of a good photometric model. If we always obtain data nadir-pointed, we will have a limited range of emission angles represented in the collected data.
- The developers of this model understand that observations will be collected by slewing (not flying) the spacecraft to look north and south at each Equatorial Station of the Detailed Survey, and this will be important to collecting a wide range of incidence and emission angles.
- We also understand that pointing knowledge uncertainties indicate that we may obtain a range of phase angles that are close to, but not equal to those planned for Detailed Survey, and this is fine. We do not need all of our data to come from exactly the same phase angle - a range of values is preferred.
- Another aspect of the flight plan that is important for this data product is the fairly uniform range to the surface - about 4.75 km during Detailed Survey. This ensures that the data are roughly of the same spatial resolution. Because a photometric model is a description of how the surface scatters light, we would expect different models for very different spatial resolution. Hence, we prefer a more limited range of values for the spatial resolution.

When in the DRM are the observations that make the data product scheduled to be taken?

The schedule below shows the DRM Rev C plans for model production and delivery (associated data products are included).

How long does it take to produce the data product?

It will take one human working full time, three weeks to produce and test photometric models for the Detailed Survey OVIRS data set. This includes, roughly speaking in the right chronological order:

- 1) Data Selection -> Spectral Photometric Data Information File (SPDIF) creation
- 2) Model creation
- 3) Model iterations
- 4) Model Testing and Validation

Is this product used for sample site selection, science value, or long-term science?

All of the above

Sample site selection

Science value

Long term science.

Data Product Structure and Organization

What is the structure of the data product?

FITS file with 2 image extensions:

FITS File Image extensions that contain the photometric model parameters for each wavelength as 2-D arrays. The first dimension (X) is the channel number (associated elsewhere with a unique wavelength), and the second dimension (Y) are the model parameters. The primary image array contains the Lommel-Seeliger model and the secondary image extension contains the ROLO model parameters. The Tertiary image extension contains the Minnaert Model parameters. For each of the models, the X^2 (chi-squared value) of the fit is the first parameter. The FITS file that will contain all the best fit models for the global OVIRS observations of Bennu will be named (for example) "Bennu_Parameters.FITS", and the user who creates this file will identify (visually - by examination of representative channels - of the .ps files that are automatically output at the conclusion of each model run) by name, the BEST of the best fit models, and record it in the FITS file keyword "MNBEST".

For example:

Model: ROLO

Order: 4th(phase function) + an exponential term(opposition surge)

Per channel:

Best Fit Metric: Chi-squared value of the best fit model

Model Coefficients: (seven free parameters): C0, C1, A0, A1, A2, A3, A4

Data Format Descriptions

Metadata and SPICE information required for each OVIRS spectrum (or Spot) as inputs to this data product: All of the following information must be captured in the SPDIF, the Spectral Photometric Data Information File for each channel:

- SCLK (time stamp of each OVIRS spectrum - each Spot)
- Spectral data (channels 1 - 1400)
- Spectral data uncertainties (channels 1 - 1400)
- Lat/Lon of the bore site
- Spatial resolution
- Range from the Sun
- Incidence angle - the angle between the sun (illumination source) and the surface normal (the surface normal is defined at the point of intersection of the bore site of the instrument with the surface of the asteroid)
- Emission angle - the angle between the surface normal (the surface normal is defined at the point of intersection of the bore site of the instrument with the surface of the asteroid) and the line (or ray) connecting the bore site of the instrument with the surface normal point.
- Phase angle - the angle between the incident ray and the emitted ray. When the surface normal, the incidence angle, and the emission angle are all co-planar, the phase angle is the sum of the incidence and the emission angles.

Information to be saved and recorded in the Modelling output file "Bennu_Parameters.FITS"

- SPDIF - Spectral Photometric Data Information File - List of Spectra used to derive Photometric Models
- List of data file selection criteria
- Optimization method used in developing the Photometric Model
- Version Number
- Creation Date
- Person who generated the Photometric Model
- Name of the model showing best fit - keyword MNBEST - for "Model Name Best"
- Location for the "Goodness of Fit" plots of the BEST fit model

Data Product Generation

How and by whom is the product generated?

How: The model is determined by fitting our equations to the data (I/F), which must be measured at a wide range of observing viewing angles (incidence, emission, and phase) in order to constrain the model parameters (equation coefficients).

By Whom: Beth Clark, Jian-Yang Li, and/or Driss Takir

What other information should be recorded?

- o Flags: limb, terminator, calibrated (0,1)
- o Fill Factor (%)
- o Range to Target (m): central pixel
- o Range from Target to Sun (km): central pixel
- o Integration time (ms)
- o All SPICE Files and Shape Models used to determine above

Are there format expectations for the input products?

Yes, the data going into the photometric model must be formatted in the form of a file we call the "SPDIF" format - Spectral Photometric Data Information File or the "IPDIF format - Imaging Photometric Data Information File. This is a file containing the SCLK-tagged spectral or imaging data, the associated uncertainties, the viewing geometry, the illumination geometry, and the spatial resolution of each spectrum selected for input to the model. Data selections are made based on quality, on fill factor, on rejection of limbs or terminators, and on the basis of very high (greater than 80 degrees) illumination and viewing angle values.

The output data product is a compilation of the 3 model fits, including an identification of the BEST model - to be determined by the modeler. For most purposes, the FITS file format will be appropriate for output of the models. In particular, we have agreed to provide a FITS file in the format described below.

- For Delivery to the PDS: Output will be FITS files, specifically formatted to conform to the SAWG data processing consensus (and PDS compliant) format (Version 8 recorded in the file named "2015_12_17_SAWG_Data_Formats_V8_VEH.xlsx"):

Key Word	Value	Description
SIMPLE	T	Conforms to FITS Standard
BITPIX	-32	8 unsigned int, 16 & 32 int, -32 & -64 real
NAXIS	2	Number of axes
NAXIS1	1400	Fastest changing axis (x) Channels
NAXIS2	16,100	Next fastest changing axis (y) spectra
EXTEND	T	FITS dataset may contain extensions
Comment	Mission Information	
MISSION	'OSIRIS-REx'	Mission: OSIRIS-REx
HOSTNAME	'OREX'	PDS Terminology
INSTRUM	'OVIRS'	Instrument: OSIRIS-REx Visible Infrared Spectrometer
TARGET	'101955 BENNU'	Target Object
ORIGIN	'OREXSPC'	University of Arizona Science Processing and Operations Center
Comment	Observation Information	
MPHASE	'Detailed Survey'	Mission Phase
ACTIVITY	'Instrument Data Collection'	Activity is equivalent to PDS4 'Primary Results Summary'
ATLTGTID		ATL Target ID (Target spacecraft is moving toward?)
SCISEQID		Instrument Phase Activity Description Rev
SEQDESC		From Description field of Science Sequence ID
OBSID		From Telemetry
Comment	Timing Information	
OBSSTART		Observation sequence start time (YYYY-MM-DDTHH:MM:SS.ssssZ)
OBSEND		Observation sequence end time.
SCLKSTRT		TICKS
SCLKEND		TICKS
Comment	Processing Info	
GEOFILE		Name of associated GEOGEN FILE
PXTOWAV		Name of pixel bin to wavelength file (changes with time)
WVLNGTHS		Name of file containing the wavelengths (does not change with time)
MNBEST	'Lommel-Seeliger'	Name of Photometric Model (Lommel-Seeliger, Minnaert, ROLO)
PHTMODFL	'Phot_Mod_LS_Bennu_Global_DS'	Name of Best Fit Photometric File containing the Model above, that was used to Photometrically correct the data (if blank, then the data have not been photometrically corrected)
SPDIF	'Bennu Global DS SPDIF.FITS'	Name of file containing the spectra used to derive Photometric Models
SPECTYP		Type of Spectrum (i.e Subsampled to Standard Grid (GRID), Thermal excess removed (NOTHERM), 1 over F (I_O_F), Phot_corr_I_OF, Bond albedo (BOND), or SPDIF)
Comment	Thermal Excess Removal Processing Info	
PLANE1	'Thermally Corrected Radiance'	Type of output
IN FILE		Name of input file
IN TEMP		Input OVIRS temperature
THERMEX	'Planck Radiation using OTES Temp'	Method of Thermal Excess Removal
IDL VER		IDL version used by Thermal Excess Removal
OS NAME		OS Version used by Thermal Excess Removal
SYSARCH		System architecture used by Thermal Excess Removal
Primary Data Unit	SPECTRAL SEQUENCE	2D array: intensity (columns) x number of spectra (rows)
2nd HDU		
XTENSION	'IMAGE '	2d.array
BITPIX		8 unsigned integer, 16 & 32 integer, -32 & -64 real
NAXIS		2 Number of Axis
NAXIS1	1400	Number of columns in image
NAXIS2	16100	Rows in image
PCOUNT		0 Mandatory FITS Keyword
GCOUNT		1 Mandatory FITS Keyword
Secondary Data Unit	SPECTRAL SEQUENCE	2D array: intensity_error (columns) x number of spectra (rows)

In addition, the input data file needs to have the correct SPICE-derived (e.g. via SpatialGen) information stored in the Binary Table extension of the above file. This table should include all relevant information per spectrum (per spot). Pointing information is relative the bore site of the OVIRS instrument.

4th HDU		
XTENSION	'BINTABLE'	Binary Table Extension
BITPIX		8 8-bit bytes
NAXIS		2 2-dimensional binary table
NAXIS1		32 width of table in bytes
NAXIS2	16,100	number of rows in table
PCOUNT		0 size of special data area
GCOUNT		1 one data group (required keyword)
TFIELDS		8 Number of fields in each row
TTYPE1	'SCLK'	label for field 1
TFORM1	'51A'	data format of field: 4-byte REAL
TUNIT1	'ticks'	Physical Unit of field
TTYPE2	'LAT'	label for field 2
TFORM2	'1E'	data format of field: 4-byte REAL
TUNIT2	'deg'	physical unit of field
TTYPE3	'LON'	label for field 3
TFORM3	'1E'	data format of field: 4-byte REAL
TUNIT3	'deg'	physical unit of field
TTYPE4	'INCIDENCE'	label for field 4
TFORM4	'1E'	data format of field: 4-byte REAL
TUNIT4	'deg'	physical unit of field
TTYPE5	'EMISSION'	label for field 5
TFORM5	'1E'	data format of field: 4-byte REAL
TUNIT5	'deg'	physical unit of field
TTYPE6	'PHASE'	label for field 6
TFORM6	'1E'	data format of field: 4-byte REAL
TUNIT6	'deg'	physical unit of field
TTYPE7	'SPATIAL_RESOLUTION'	label for field 7
TFORM7	'1E'	data format of field: 4-byte REAL
TUNIT7	'm/pix'	physical unit of field
TTYPE8	'RANGE TO SUN'	label for field 8
TFORM8	'1E'	data format of field: 4-byte REAL
TUNIT8	'km'	physical unit of field

What algorithms and/or calibration data are used to generate products?

The photometric models will follow the Minnaert, Lommel-Seeliger, and ROLO equations as described in the literature. For a more complete description, see Takir et al. 2015 (linked below), or the associated Algorithm Description.

Our photometric modeling software uses the MPFIT() (IDL built-in function) Optimization method.

Has a specific Science Team Member been assigned to produce this product?

Beth Ellen Clark has been assigned with this data product. She will work with Jian-Yang Li, and Driss Takir to complete the work and close out the requirements.

Will multiple versions of the product be generated?

Possibly, but not during proximity operations. At that time, the plan is to deliver a 4-station empirical model for the purposes of site selection. Later on, for longer term science, other photometric models may be created or used.

Data Product Validation

How will the product be vetted to ensure contents and format are correct?

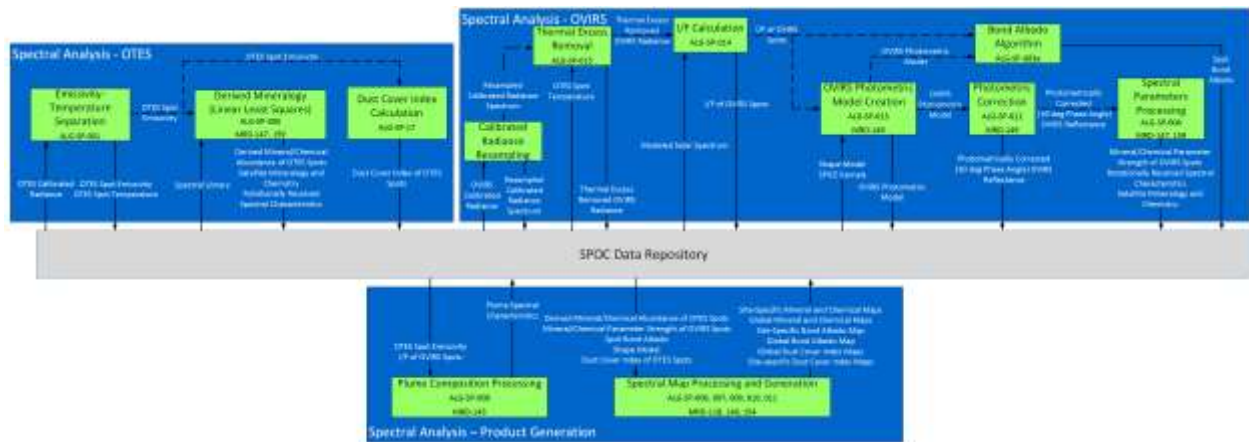
Goodness of fit & chi-squared will provide a measure of success of the modeling effort and a way to compare various possible models for selection of the “Best” fit model. We will check the following plots: (I/F)modeled vs. (I/F)measured, ratio (I/Fmodeled / I/Fmeasured) vs. incidence, ratio (I/Fmodeled / I/Fmeasured) vs. emission and ratio (I/Fmodeled / I/Fmeasured) vs. phase angle.

The general approach (including which models) has been vetted and validated by consulting with experts: Jian-Yang Li (who is now a collaborator).

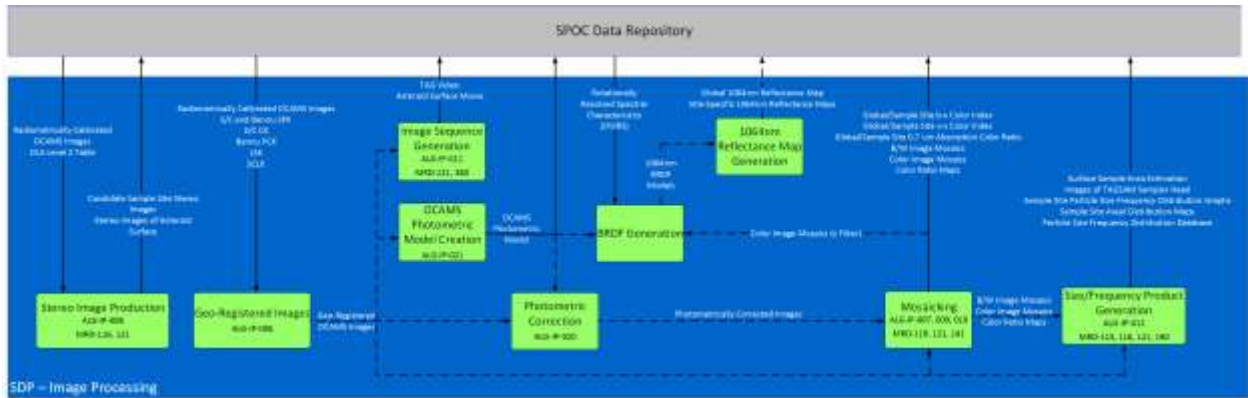
Data Flow

Rough Overview of the Data Flow organized chronologically:

This figure shows how Photometric Modeling and the subsequent Photometric Correction fit into the SPOC Overview of the Spectral Analysis Data Flow, organized structurally:



This figure shows how Photometric Modeling and the subsequent Photometric Correction fit into the SPOC Overview of the Image Processing Data Flow, organized structurally:



Describe the sources, destinations, and transfer procedures for data products:

Each Photometric Model set will be stored in the SPOC Data Repository, and a Best Fit model will be identified by the creator (e.g. of the file "Bennu_OVIRS_Parameters.FITS" file). The best fit model will be stored in the "MNBEST" (Model Name Best) keyword in the header information (e.g. Lommel-Seeliger).

State the size of an individual data product and the total size of all the data products generated over the course of each mission phase.

See the above description.

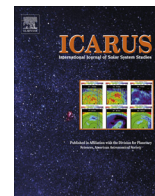
Most recently reviewed by Jian-Yang Li and Beth Clark on 2016-03-30.

Photometric Modeling Schedule

V9

Beth Ellen Clark

	Instrument / Data	Downlink of Data	Staffing Plan	Delivery of Photometric Model	Delivery of Phot Corrected Data	Delivery of Associated Data Products	Comments
Approach	OVIRS	10/31/18	BEC, XDZ			11/7/18	Global Scale Factor for 1064nm/860nm Disk-integrated model update only
	MapCam	11/5/18	JYL, DT	11/22/18			
Preliminary Survey	MapCam	11/29/18	XDZ, BEC ?				
	PolyCam	11/29/18	DT, JYL ?				
Orbital A	OVIRS	12/24/18					
	NavCam	1/9/19					
Detailed Survey	PolyCam	1/25/19					very limited viewing geometry in Baseball Diamond: 10am & 2pm - will provide MapCam panchrom model when available for photometric correction of these data.
	MapCam Pan	2/25/19	DT, XDZ	3/18/19	3/21/19		
	MapCam X	2/25/19	DT, BEC	3/25/19	3/28/19	4/5/19	
	OVIRS	2/25/19	JYL, XDZ	3/18/19	3/21/19	3/28/19	
	MapCam Color	2/25/19	BEC, JYL	4/2/19	4/5/19	4/14/19	
Orbital B	PolyCam	5/1/19					
	NavCam	5/12/19					
Reconnaissance	PolyCam	5/28/19 - 8/26/19					Recon Data will be corrected with the Photometric Models developed from Detailed Survey Data. There are 6 RECON data downloads, spread over 3 months. (Note: Because of the limited lighting geometry available in the PolyCam dataset, it is not possible to photometrically model the PolyCam data. Instead, the MapCam panchrom filter model will be used.)
	MapCam	5/28/19 - 8/26/19			1 day after each downlink		
	OVIRS	5/28/19 - 8/26/19			1 day after each downlink		
DRM Rev C	Data Downlinked and shaded grey will not be photometrically modeled in the Baseline plan.						



Photometric models of disk-integrated observations of the OSIRIS-REx target Asteroid (101955) Benu



Driss Takir^{a,c,*}, Beth Ellen Clark^a, Christian Drouet d'Aubigny^b, Carl W. Hergenrother^b, Jian-Yang Li^c, Dante S. Lauretta^b, Richard P. Binzel^d

^a Department of Physics and Astronomy, Ithaca College, Ithaca, NY 14850, USA

^b Lunar and Planetary Laboratory, University of Arizona, 1629 E. University Blvd., Tucson, AZ 85721, USA

^c Planetary Science Institute, 1700 E. Ft. Lowell Road, Suite 106, Tucson, AZ 85719, USA

^d Massachusetts Institute of Technology, 77 Massachusetts Avenue, Cambridge, MA 02139, USA

ARTICLE INFO

Article history:

Received 19 November 2014

Revised 1 February 2015

Accepted 3 February 2015

Available online 10 February 2015

Keyword:

Photometry

Asteroids

Near-Earth objects

ABSTRACT

We used ground-based photometric phase curve data of the OSIRIS-REx target Asteroid (101955) Benu and low phase angle data from Asteroid (253) Mathilde as a proxy to fit Benu data with Minnaert, Lommel-Seeliger, (Robotic Lunar Orbiter) ROLO, Hapke, and McEwen photometric models, which capture the global light scattering properties of the surface and subsequently allow us to calculate the geometric albedo, phase integral, spherical Bond albedo, and the average surface normal albedo for Benu. We find that Benu has low reflectance and geometric albedo values, such that multiple scattering is expected to be insignificant. Our photometric models relate the reflectance from Benu's surface to viewing geometry as functions of the incidence, emission, and phase angles. Radiance Factor functions (RADFs) are used to model the disk-resolved brightness of Benu. The Minnaert, Lommel-Seeliger, ROLO, and Hapke photometric models work equally well in fitting the best ground-based photometric phase curve data of Benu. The McEwen model works reasonably well at phase angles from 20° to 70°. Our calculated geometric albedo values of $0.047_{-0.014}^{+0.012}$, $0.047_{-0.014}^{+0.005}$, and $0.048_{-0.022}^{+0.012}$ for the Minnaert, the Lommel-Seeliger, and the ROLO models respectively are consistent with the geometric albedo of 0.045 ± 0.015 computed by Emery et al. (Emery, J.P. et al. [2014]. Icarus 234, 17–35) and Hergenrother et al. (Hergenrother, C.W. et al. [2014]. <<http://arxiv.org/abs/1409.4704>>). Also, our spherical Bond albedo values of $0.016_{-0.004}^{+0.005}$, $0.015_{-0.001}^{+0.003}$, and $0.015_{-0.005}^{+0.007}$ for the Minnaert model, Lommel-Seeliger, and ROLO models respectively are consistent with the value of 0.017 ± 0.002 presented by Emery et al. (Emery, J.P. et al. [2014]. Icarus 234, 17–35). On the other hand, the semi-physical models such as the Hapke model, where several assumptions and approximations were necessary, and the McEwen model are not supported by the global disk-integrated data, indicating that disk-resolved measurements will be necessary to constrain these models, as expected.

© 2015 Elsevier Inc. All rights reserved.

1. Introduction

Near-Earth Apollo Asteroid (101955) Benu (provisional designation 1999 RQ₃₆) is under intense scrutiny because it is the target of the NASA Origins Spectral Interpretation Resource Identification Security Regolith Explorer (OSIRIS-REx) mission (Clark et al., 2011; Nolan et al., 2013; Hergenrother et al., 2013, 2014; Emery et al., 2014; Chesley et al., 2013). The OSIRIS-REx spacecraft will collect a sample of Asteroid Benu and return to Earth in 2023 (Lauretta et al., 2015).

The primary objective of OSIRIS-REx is to return pristine samples of carbonaceous material from the surface of a primitive asteroid. The target asteroid, near-Earth object Benu, is an accessible volatile and organic-rich remnant from the early Solar System. OSIRIS-REx returns a minimum of 60 g of bulk regolith and a separate 26 cm² of fine-grained surface material from this body. Analyses of these samples provides knowledge about presolar history, from the initial stages of planet formation to the origin of life. Prior to sample acquisition, OSIRIS-REx will perform comprehensive global mapping of the topography, mineralogy, and chemistry of Benu, resolving geological features, revealing its geologic and dynamic history, and providing context for the returned samples. The instruments will also document the regolith

* Corresponding author at: Department of Physics and Astronomy, Ithaca College, Ithaca, NY 14850, USA. Fax: +1 607 274 1773.

E-mail address: dtakir@ithaca.edu (D. Takir).

at the sampling site in situ at scales down to the sub-centimeter. In addition, OSIRIS-REx will study the Yarkovsky effect, a non-Keplerian force affecting the orbit of this potentially hazardous asteroid (PHA), and will provide ground truth measurements for telescopic observations of carbonaceous asteroids.

We present photometric models constrained by disk-integrated asteroid brightness data, which predict the disk-resolved brightness of Asteroid Benu. These models provide Bidirectional Reflectance Distribution Functions (*BRDFs*) for this asteroid; functions of this form provide important information to scientists and engineers designing OSIRIS-REx instruments. In order to model Benu's surface brightness, we have selected three photometric models: the Minnaert model (Minnaert, 1941), the Lommel-Seeliger model (Seeliger, 1884), and the RObotic Lunar Orbiter (ROLO) model (Buratti et al., 2012). With these models, the geometric albedo, the phase integral, the spherical Bond albedo, and the normal albedo can be computed for Benu. The spherical Bond albedo is an important quantity to constrain the thermal properties of Benu, relevant to estimates of thermal inertia and models of the Yarkovsky effect (Emery et al., 2014; Chesley et al., 2013).

The OSIRIS-REx spacecraft will observe Benu at a wide range of viewing geometries, and our photometric models are useful for predicting flux and brightness quantities at these geometries. We used ground-based disk integrated data (Hergenrother et al., 2013) to constrain possible disk-resolved photometric behavior. Because there are a variety of disk-resolved scattering laws that can mimic the same disk-integrated data, our models are uncertain and preliminary, and will be updated when the spacecraft arrives at Benu. Because of the wide range of models that are consistent with the limited available data, we estimate the error envelope of our predictions, and provide minimum and maximum expected diversions in brightness that may be observed at the surface of Benu.

2. Methodology

We used the mean diameter of Benu from Nolan et al. (2013) in our photometric models: 0.492 ± 0.020 km, and the calibrated ground-based photometric phase curve data from Hergenrother et al. (2013). All lightcurve and phase functions of Benu observations were acquired during the 2005–2006 and 2011–2012 apparitions. Most of the optical magnitudes were not corrected for rotational modulation. Only the 4 nights from September 2005 were corrected as the data were taken specifically for lightcurve work. Because the low lightcurve amplitude of ± 0.15 magnitudes was comparable to the photometric uncertainty most nights, Hergenrother et al. (2013) increased the errors for that data to also take into account lightcurve effects.

In our nominal model, the reduced V magnitude (the apparent visual magnitude with influence of distance removed) values include the NEAR spacecraft data of Mathilde (Clark et al., 1999). We are using Mathilde data as the best available proxy because ground-based observations of Benu are lacking data at the low and high ends of the phase angle range.

The maximum model was computed (using V magnitude $- 1\sigma$ uncertainty), and the minimum model was computed (using V magnitude $+ 1\sigma$ uncertainty). The maximum and minimum models capture the scatter in the moderate phase angle ground-based observations of Benu, the uncertainties in the mean diameter (0.492 ± 0.020), and the low and high phase-angle behavior. To compute our model best-fit parameter sets, we used the Interactive Data Language (IDL) MPFIT package, which uses a Levenberg–Markwardt (LM) least-squares minimization algorithm (MINPACK-1) (Markwardt, 2008). The LM algorithm is based on the Gauss–Newton and the gradient descent methods, and requires a good initial estimate of the model parameter sets. Some of these

model parameters are directly related to the geometric albedo (Section 2.3). Therefore, knowing the geometric albedo for B-type asteroids can help choose the appropriate initial values for the model fitting.

2.1. Model BRDFs and RADFs for Benu

Radiance Factor (*RADF*) is the ratio of the bidirectional reflectance of a surface to that of a perfectly diffuse surface illuminated at $i = 0^\circ$ (Hapke, 2012). Bidirectional Reflectance Distribution Function (*BRDF*) is the ratio of the radiance scattered by a surface into a given direction to the collimated power incident on a unit area of the surface (Hapke, 2012). Functions in the form of *BRDFs* are requested by the OSIRIS-REx instrument teams to be used to predict the returned flux from Benu and its brightness during the different observing campaigns of the mission, in particular, the quantity *RADF*, or $[I/\mathcal{F}](i, e, a)$ (reflectance) of Benu is of most interest. Therefore, we present our Minnaert, Lommel-Seeliger, and ROLO, modeled *BRDF* for use in predicting the reflectance of Benu. *BRDF* is directly related to *RADF* and bidirectional reflectance, r , as described in the following sections (Hapke, 2012).

2.1.1. Minnaert model

Minnaert's model is a generalization of Lambert's law, suggested by Minnaert (1941). Li et al. (2009) added an empirical phase function term, which describes the variation in surface reflectance with phase angle (a) (in degrees), to the model: $f(a) = 10^{-\frac{ba}{25}}$ (linear-magnitude). The phase function of Li et al. (2009) did not work well in fitting Benu data so we further modified it as follows:

$$f(a) = 10^{-\frac{(ba+ca^2+da^3)}{25}} \quad (\text{polynomial-magnitude}). \quad (1)$$

The Minnaert model has six free parameters and includes the effects of limb-darkening and the surface phase function:

$$\begin{aligned} BRDF(i, e, a) &= \frac{RADF(i, e, a)}{I_o p} = \frac{[I/\mathcal{F}](i, e, a)}{I_o p} = \frac{Pr(i, e, a)}{I_o p} \\ &= A_M f(a) (I_o I)^{k(a)-1}, \end{aligned} \quad (2)$$

where $I_o = \cos(i)$, $I = \cos(e)$, i is the incidence angle (degrees), e is the emission angle (degrees). A_M is the Minnaert albedo, $k(a) = k_o + ba$ characterizes the limb-darkening behavior of the surface, and b captures the linear relationship between k and phase angle (a). k_o is the value of k at zero degree phase angle. I is the radiance and has units of $W/m^2/sr$. $J = p\mathcal{F}$ is the collimated light (irradiance) and has units of W/m^2 . Strictly speaking I/\mathcal{F} is a dimensionless quantity (\mathcal{F} has units of $W/m^2/steradian$ and p here has units of steradian). *RADF*(I/\mathcal{F}) is what is measured by the spacecraft.

2.1.2. Lommel-Seeliger model

Lommel-Seeliger's model was originally developed by Seeliger (1884) and modified by Hapke (2012). In order to better fit Benu data, we added an exponential empirical phase function term to this model:

$$f(a) = e^{ba+ca^2+da^3}, \quad (3)$$

which describes the variation in surface reflectance with phase angle (a). The Lommel-Seeliger model has four free parameters and includes the effects of limb-darkening and the surface phase function:

$$BRDF(i, e, a) = A_{LS} \frac{f(a)}{I_o + I}, \quad (4)$$

where $A_{LS} = \frac{A_o}{4p}$ is the Lommel-Seeliger albedo and I_o is the average particle single scattering albedo.

2.1.3. ROLO model

The ROLO model was developed by Buratti et al. (2012), using the United States Geological Survey's ROLO data from NASA's Moon Mineralogy Mapper (M^3). The ROLO model describes the lunar scattering law, given by the $\frac{f(a)}{p(1+\Gamma)}$ term (often called the Lommel-Seeliger function), and was derived from the equation of radiative transfer (Chandrasekhar, 1960). The ROLO model has seven free parameters and includes the effects of limb-darkening and the surface phase function:

$$BRDF(i, e, a) = \frac{f(a)}{p(1+\Gamma)}, \quad (5)$$

the phase function $f(a) = C_0 e^{-C_1 a} + A_0 + A_1 a + A_2 a^2 + A_3 a^3 + A_4 a^4$ includes an exponential term that describes the opposition surge.

2.2. Bennu disk-integrated brightness

Solving for $r(i, e, a)$, which is directly related to $[I/\mathcal{F}](i, e, a)$, for the models described in the previous section, the following disk-resolved function can be integrated to give the disk-integrated magnitude of Bennu. We start with the disk-averaged albedo, $A(a)$, as a function of phase angle, assuming a spherical shape:

$$A(a) = \int_{h=p/2}^{-p/2} \int_{\prime=a-p/2}^{p/2} r(i, e, a) |\cos(h)| d\prime dh, \quad (6)$$

where h is the photometric latitude (the angle between the normal to the surface and the scattering plane), and \prime is the photometric longitude (the angle in the scattering plane between projection of the normal and direction from the object to the observer). The disk-integrated absolute magnitude is then a function of the disk-averaged albedo (Pravec and Harris, 2007):

$$H(a) = -5 \log_{10} \left(\frac{D \sqrt{A(a)}}{K} \right), \quad (7)$$

where D is Bennu's mean diameter in (km), and $K \equiv 2 \text{ AU} \times 10^{V_{\text{Sun}}/5}$ with the V magnitude of the Sun $V_{\text{Sun}} = -26.762 \pm 0.017$ (Campins et al., 1985).

2.3. Geometric albedo

Physical albedo (a.k.a., geometric albedo) (A_{geo}), which is a disk-integrated quantity, is the ratio of the brightness of a body observed from zero phase angle $a = 0^\circ$ to the brightness of a perfect Lambert (flat) disk of the same radius and at the same distance as the body, but illuminated and observed along an axis perpendicular to the plane of the disk (Hapke, 2012). The geometric albedo is usually presented at one wavelength, the V passband, centered around $0.55 \mu\text{m}$:

$$A_{\text{geo}} = \int_{2p} \frac{REFF(e, e, 0)}{p} |I|_o dX, \quad (8)$$

where $dX = 2p \sin(e) de = -2p dl$ and the Reflectance Factor (or reflectance coefficient) ($REFF$) is the ratio of the reflectance of the surface to that of a perfectly diffuse (Lambert) surface under the same conditions of illumination. $REFF$ is defined as follows:

$$REFF(i, e, a) = \frac{[I/\mathcal{F}](i, e, a)}{|I|_o}. \quad (9)$$

This reflectance quantity ($REFF$) is what is generally measured in the laboratory. For OSIRIS-REx Visible-Infrared Spectrometer (OVIRS) (Reuter and Simon-Miller, 2012; Simon-Miller and Reuter, 2013) mineralogic spectral indices, the spacecraft measurements will be photometrically corrected to a standard viewing geometry ($i = 30^\circ$,

$e = 0^\circ$, $a = 30^\circ$) in $REFF$ units for comparison with standard reference mineral libraries.

Disk-resolved scattering models can be used to compute the derived quantities of geometric albedo, using equations in Section 2.3 and Eqs. (8) and (9).

Minnaert geometric albedo:

$$\begin{aligned} A_{\text{geo}} &= 2p A_M f(0) \int_0^{p/2} [\cos(e)]^{2k_0} \sin(e) de \\ &= A_M \frac{2p}{2k_0 + 1} f(0), \end{aligned} \quad (10)$$

where $f(0)$ is the Minnaert phase function at $a = 0^\circ$.

Lommel-Seeliger geometric albedo:

$$A_{\text{geo}} = \frac{A_{LS}}{2} p f(0) \int_0^{p/2} \cos(e) \sin(e) de = \frac{A_{LS}}{2} p f(0), \quad (11)$$

where $f(0)$ is the Lommel-Seeliger phase function at $a = 0^\circ$.

ROLO geometric albedo:

$$A_{\text{geo}} = f(0) \int_0^{p/2} \cos(e) \sin(e) de = \frac{f(0)}{2}, \quad (12)$$

where $f(0)$ is the ROLO phase function at $a = 0^\circ$.

2.4. Spherical Bond albedo

Spherical Bond albedo (a.k.a., Bond albedo) (A_{sph}) is the total fraction of incident irradiance scattered by a body into all directions at one wavelength, usually presented for $0.55 \mu\text{m}$ (Hapke, 2012):

$$A_{\text{sph}} = \frac{1}{p} \int_{2p} \int_{2p} r(i, e, a) |dX_i dX_e|, \quad (13)$$

where $dX_i = \sin(i) di dw$ and $dX_e = \sin(e) de dw$ with w is the azimuth.

The spherical Bond albedo can also be expressed as $q A_{\text{geo}}$, where q is the phase integral, defined as:

$$q = 2 \int_0^p U(a) \sin(a) da, \quad (14)$$

where $U(a) \equiv \frac{F(a)}{F(0^\circ)}$ is the disk-integrated brightness at phase angle a , assuming a spherical body (Buratti and Veverka, 1983). $F(a)$ is the phase dependence of the disk-integrated flux defined as follows:

$$F(a) = \frac{D^2}{4r^2} \int_{-\frac{p}{2}}^{\frac{p}{2}} \int_{a-\frac{p}{2}}^{\frac{p}{2}} [I/\mathcal{F}](i, e, a) \cos(\prime) \cos^2(h) d\prime dh, \quad (15)$$

where $\prime = \text{Arctan} \left[\frac{\cos(i)}{\cos(e)} - \cos(a) \right]$ is the photometric longitude, $h = \text{Arccos} \left[\frac{\cos(e)}{\cos(\prime)} \right]$ is the photometric latitude, D = diameter of Bennu, and r = observer-Bennu distance.

Bolometric Bond albedo (A_{bolo}) is the average of the spherical Bond albedo $A_{\text{sph}}(k)$ weighted by spectral irradiance of the Sun $J_S(k)$. This integrates spherical albedo over all k (Hapke, 2012):

$$A_{\text{bolo}} = \frac{\int_0^\infty A_{\text{sph}}(k) J_S(k) dk}{\int_0^\infty J_S(k) dk}. \quad (16)$$

The OSIRIS-REx Science Team has adopted a composite solar flux model from Thuillier et al. (2003) and Rieke et al. (2008), which ranges from $\sim 0.435 \mu\text{m}$ to $1.8 \mu\text{m}$. The bolometric Bond albedo is the quantity required for estimates of thermal inertia and models of the Yarkovsky effect for OSIRIS-REx for Asteroid Bennu.

It is generally assumed that the spherical Bond albedo in the V passband ($\sim 550 \text{ nm}$) is a good representation of the bolometric

Bond albedo. This is because most of the Sun's energy is in the visible and most spectra of Solar System bodies do not change drastically over the UV/visible spectral range.

2.5. Normal albedo

The normal albedo (A_n) is defined as the ratio of the brightness of a surface observed at zero phase angle from an arbitrary direction to the brightness of a perfectly diffuse surface located at the same position, but illuminated and observed perpendicularly (Hapke, 2012).

$$A_n = \text{pr}(e, e, 0). \quad (17)$$

At $i = e = 0^\circ$, the normal albedo is equivalent to the geometric albedo for Lommel-Seeliger surfaces (Lester et al., 1979).

3. Results

Using the Minnaert, Lommel-Seeliger, and ROLO RADF functions described in the previous section, we constrained the average disk-resolved brightness across the surface of Bennu by fitting the disk-integrated ground-based phase curve of this asteroid from Hergenrother et al. (2013). Tables 1a, 1b, and 1c show our Minnaert, Lommel-Seeliger, and ROLO models, respectively, for nominal, maximum, and minimum predicted brightness of Bennu at 550 nm.

The minimum and maximum models capture the uncertainties in the size of Bennu, its low and high phase-angle behavior, and the scatter in the moderate phase angle ground-based observations of Bennu. Using the Minnaert, Lommel-Seeliger, and ROLO models, we computed minimum, maximum, and nominal geometric albedo (A_{geo}), phase integral (q), and spherical albedo (A_{sph}) for Bennu (Table 2). The calculated geometric albedo.

Figs. 1–3 show the data for Bennu as compared with our models. We note that the BRDF values at $i = 0^\circ$, $e = 0^\circ$, and $a = 0^\circ$, calculated using our Minnaert, Lommel-Seeliger, and ROLO models are $0.012^{+0.000}_{-0.001}$, $0.015^{+0.002}_{-0.005}$, and $0.015^{+0.002}_{-0.005}$, respectively.

The Lommel-Seeliger BRDF value represents almost $1/p$ times the geometric albedo: 0.045 ± 0.015 as expected for Lommel-Seeliger spheres (Lester et al., 1979). Table 2 includes the calculated Bennu geometric albedo, phase integral, spherical Bond albedo, and normal albedo values for the Minnaert, Lommel-Seeliger, and ROLO models. These values are consistent with the geometric albedo, phase integral, and spherical Bond albedo values calculated by Hergenrother et al. (2013, 2014) and Emery et al. (2014), who combined Bennu's thermal IR and visible phase function properties.

The calculated geometric albedo values were found to be $0.047^{+0.012}_{-0.014}$, $0.047^{+0.005}_{-0.014}$, and $0.048^{+0.012}_{-0.022}$ for the Minnaert, the Lommel-Seeliger, and the ROLO models respectively. In comparison with other dark objects, the geometric albedo values for Mathilde (Clark et al., 1999), Phobos (Simonelli et al., 1998), and Deimos (Simonelli et al., 1998) were found to be 0.047 ± 0.005 , 0.071, and 0.068 respectively.

Table 1a
Minnaert functions that predict $[I/\mathcal{F}](i, e, a)$ (reflectance) of Bennu at 550 nm.

	A_M^a	b^b	c^b	d^b	k_o	b
Nominal	0.012	0.045	-2.50×10^{-4}	7.76×10^{-7}	0.30	0.002
Maximum	0.012	0.034	4.79×10^{-5}	-1.12×10^{-6}	0.15	0.001
Minimum	0.011	0.044	-2.86×10^{-4}	9.15×10^{-7}	0.55	0.003

^a A_M is Minnaert albedo.

^b $f(a) = 10^{-\frac{(ba+ca^2+da^3)}{25}}$. The values given in this table for b, c, and d were derived for phase angle values in units of degrees.

Table 1b
Lommel-Seeliger functions that predict $[I/\mathcal{F}](i, e, a)$ (reflectance) of Bennu at 550 nm.

	A_{LS}^a	b^b	c^b	d^b
Nominal	0.030	-4.36×10^{-2}	2.69×10^{-4}	-9.90×10^{-7}
Maximum	0.033	-2.51×10^{-2}	1.62×10^{-4}	-18.77×10^{-7}
Minimum	0.021	-4.17×10^{-2}	2.72×10^{-4}	-11.96×10^{-7}

^a A_{LS} is Lommel-Seeliger albedo.

^b $f(a) = e^{ba+ca^2+da^3}$. The values given in this table for b, c, and d were derived for phase angle values in units of degrees.

4. Discussion

We fitted three empirical photometric models (Minnaert, Lommel-Seeliger, and ROLO) to the brightness data of Bennu in order to predict how the brightness of Bennu depends on illumination and observing geometries. These three models work equally well in fitting Bennu's data. We will be using these models during the OSIRIS-REx mission operations.

For the purposes of discussion, we have also fitted the Bennu data with two other models: Hapke and McEwen (Hapke, 2012; McEwen, 1986, 1991); however, these two models will not be used during operations because they have some limitations. In this section, we will discuss the implications of these photometric models for OSIRIS-REx instrument teams.

4.1. The selected photometric models for Bennu

The Minnaert, Lommel-Seeliger, and ROLO models are well-suited for predicting the brightness of Bennu at arbitrary illumination and viewing geometries. These models are also well-suited for photometrically correcting Bennu imaging and spectral observations to a common standard geometry, and therefore, for comparing images of different areas on Bennu with each other and Bennu's spectral data with laboratory measurements. However, these models cannot be used to infer the physical properties and compositions of Bennu's surface. We chose to use these three models because they relate the reflectance from a particulate surface to viewing geometry in a simple fashion as functions of the incidence, emission, and phase angles (disk function and phase function). Furthermore, Minnaert, Lommel-Seeliger, and ROLO models work well for Bennu's very low surface reflectance and geometric albedo, where multiple scattering is not significant. Generally, planetary objects with a high surface reflectance and geometric albedo follow the Lambert law (Li et al., submitted for publication). Tables 3a and 3b show Hapke and McEwen models, respectively, which predict $[I/\mathcal{F}](i, e, a)$ of Bennu at 550 nm.

4.2. Other photometric models

4.2.1. Hapke model

The Hapke model is based on a semi-physical model that uses the analytical solutions of radiative transfer on an asteroidal surface with simplification assumptions, coupled with the empirical models that describe the scattering behavior aspects of a particulate surface (Hapke, 2012):

$$RADF(i, e, a) = \frac{-\circ}{4} \frac{1}{\circ + 1} \{ [1 + B(a)]p(a) + H(\circ)H(1) - 1 \} S(i, e, a, h), \quad (18)$$

where $-\circ$ is the average particle single scattering albedo, B is the shadow hiding opposition surge function, $p(a)$ is the average particle single-scattering phase function, H is Ambartsumian–Chandrasekhar function for multiple scattering, and S is the Hapke roughness shadowing function.

Table 1c
ROLO functions that predict $[I/\mathcal{F}](i, e, a)$ (reflectance) of Benu at 550 nm.

	C_0	C_1	A_0	A_1	A_2	A_3	A_4
Nominal	0.043	0.080	0.053	-1.04×10^{-3}	7.75×10^{-6}	-1.54×10^{-8}	-3.74×10^{-11}
Maximum	0.263	0.010	-0.14	-1.45×10^{-3}	5.14×10^{-5}	-4.67×10^{-7}	1.54×10^{-9}
Minimum	-0.022	-0.012	0.074	-9.56×10^{-4}	1.14×10^{-5}	1.16×10^{-8}	-2.42×10^{-10}

$f(a) = C_0 e^{-C_1 a} + A_0 + A_1 a + A_2 a^2 + A_3 a^3 + A_4 a^4$. The first term of the phase function describes opposition surge.

Table 2
Benu's geometric albedo, phase integral, spherical albedo, and normal albedo.

	Geometric albedo (A_{geo})	Phase integral (q)	Spherical albedo (A_{sph})	Normal albedo (A_n)
Minnaert model	$0.047^{+0.012}_{-0.014}$	$0.34^{+0.02}_{-0.03}$	$0.016^{+0.005}_{-0.004}$	$0.038^{0.000}_{-0.003}$
Lommel-Seeliger model	$0.047^{+0.005}_{-0.014}$	$0.32^{+0.00}_{-0.09}$	$0.015^{+0.003}_{-0.001}$	$0.047^{+0.006}_{-0.010}$
ROLO model	$0.048^{+0.012}_{-0.022}$	$0.32^{+0.05}_{-0.07}$	$0.015^{+0.007}_{-0.005}$	$0.047^{+0.012}_{-0.021}$

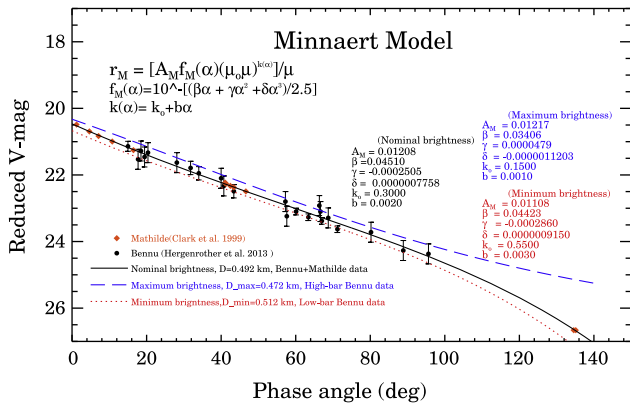


Fig. 1. The reduced V magnitude of Benu as a function of phase angle predicted by the Minnaert model is shown compared with the ground-based measurements. Shown are the minimum (red dots), maximum (blue dashes), and nominal (black solid line) models. Our minimum and maximum models do not include the Mathilde data, however our nominal model does. r_M is in units of sr^{-1} . (For interpretation of the references to color in this figure legend, the reader is referred to the web version of this article.)

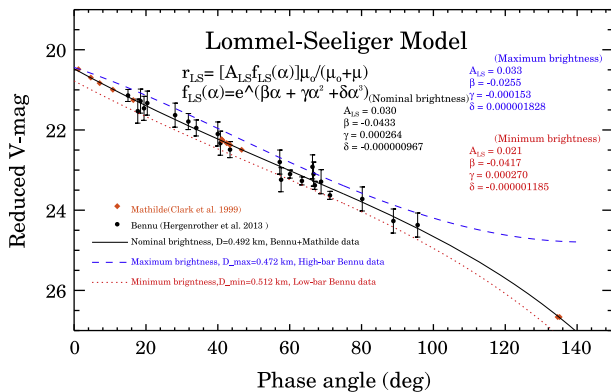


Fig. 2. The reduced V magnitude of Benu as a function of phase angle predicted by the Lommel-Seeliger model is shown compared with the ground-based measurements. Shown are the minimum (red dots), maximum (blue dashes), and nominal (black solid line) models. Our minimum and maximum models do not include the Mathilde data, however our nominal model does. r_{LS} is in units of sr^{-1} . (For interpretation of the references to color in this figure legend, the reader is referred to the web version of this article.)

Fig. 4 shows the ground-based measurements of Benu as compared with the Hapke model. Although the Hapke model is a semi-physical photometric model and fits well Benu's data, this model

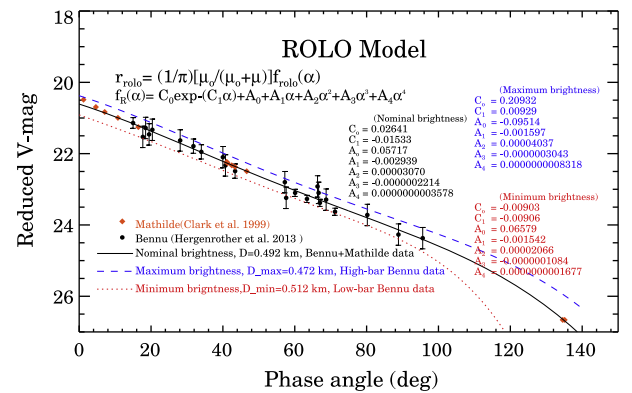


Fig. 3. The reduced V magnitude of Benu as a function of phase angle predicted by the ROLO model is shown compared with the ground-based measurements. Shown are the minimum (red dots), maximum (blue dashes), and nominal (black solid line) models. Our minimum and maximum models do not include the Mathilde data, however our nominal model does. r_{rolo} is in units of sr^{-1} . (For interpretation of the references to color in this figure legend, the reader is referred to the web version of this article.)

does not allow the computation of exact and unique solutions of radiative transfer equations of the surface physical conditions of this asteroid. In addition, the Hapke model requires making some assumptions and approximations. The limited observing geometries available from the ground-based observations, particularly at small phase angles, are insufficient to fully constrain a Hapke model; as a result, the Hapke model is not useful for interpreting Benu's disk-integrated data at this early stage of the OSIRIS-REX mission.

Because the surface roughness parameter h and the asymmetry factor g cannot be decoupled from disk-integrated phase function, we had to assume $h = 20$ and fixed it for the fitting the data. Also, we did not place any constraints (such as the $B_0 < 1$) for the opposition effect parameters. With these assumptions and approximations, the Hapke fit for Benu is not unique. This model is very difficult to apply to Benu's data because Hapke's phase function and bidirectional reflectance are not linear, and their five parameters are entangled with each other. Furthermore, Shepard and Helfenstein (2007), who compared the known characteristics of laboratory samples to those predicted by fitting of the Hapke model parameters, found that this model does not adequately describe the physical state of the samples.

4.2.2. Lommel-Seeliger–Lambert model

The Lommel-Seeliger–Lambert model (also called the lunar-Lambert model) is a hybrid model that includes a lunar scattering function, given by the $\frac{1}{r_0 + t}$ term (Seeliger, 1884), in addition to a

Table 3a
Hapke function that predicts $[I/\mathcal{F}]$ (i, e, a) (reflectance) of Benu at 550 nm.

	\bar{w}_0	B_0	h	g	\bar{h}
Hapke	0.031	3.9	0.11	-0.32	20

Table 3b
McEwen function that predicts $[I/\mathcal{F}]$ (i, e, a) (reflectance) of Benu at 550 nm.

	A_{MC}	b	c	d
McEwen	0.015	-0.043	2.66×10^{-4}	9.75×10^{-7}

Lambert disk function (Lambert, 1759) (Buratti and Veverka, 1983):

$$RADF(i, e, a) = A \frac{I_0}{I_0 + I} f(a) + B I_0, \quad (19)$$

where A, B , and f are functions of a .

This hybrid model was originally introduced by Buratti and Veverka (1983) to photometrically model the bright plains and the dark terrain of Europa. By setting $B = 1 - A$ in Eq. (19), Buratti and Veverka (1983) suggested a simple expression that spans the range between lunar-like scattering ($A = 1$), and Lambert-like scattering ($A = 0$). Bright objects with high geometric albedos are well-described by the Lambert-like scattering law, and dark objects with low geometric albedos, where multiple scattering can be negligible (like in Benu), are well described by the lunar-like scattering law. Hence, the Lommel-Seeliger–Lambert model works well for objects with a wide range of different geometric albedos such as Europa (Buratti and Veverka, 1983).

Because the Lommel-Seeliger–Lambert model cannot be applied for photoclinometry, where measurements from two profiles (two versions of Eq. (19)) cannot be ratioed to remove the effects of the intrinsic reflectivity of the surface materials, McEwen (1991, 1986) rewrote Eq. (19) in the following form:

$$RADF(i, e, a) = B_0(a) \left[\frac{2L(a)I_0}{I_0 + I} + (1 - L(a))I_0 \right], \quad (20)$$

where $L(a) = \frac{Af(a)}{Af(a)+2B}$ is a partition parameter between the Lommel-Seeliger term and the Lambert term, and $B_0(a)$ is the intrinsic albedo

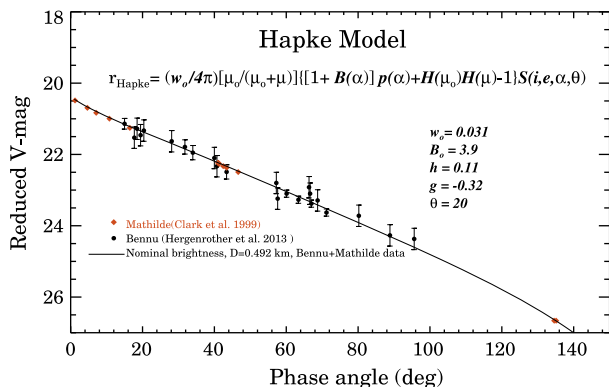


Fig. 4. The reduced V magnitude of Benu as a function of phase angle predicted by the Hapke model is shown compared with the ground-based measurements. B_0 is the shadow hiding opposition surge function, $p(a)$ is the average particle single-scattering phase function, H is Ambartsumian–Chandrasekhar function for multiple scattering, and S is the Hapke roughness shadowing function. r_{Hapke} is in units of sr^{-1} . \bar{w}_0 is the single-scattering albedo (fraction of total incident energy that is scattered by a single particle towards all directions), B_0 is the opposition effect amplitude parameter, h is the opposition effect width parameter, g is the asymmetry parameter (spatial energy distribution in a single particle scattering phase function), and \bar{h} is the surface roughness parameter (average deviation of local normal with respect to average).

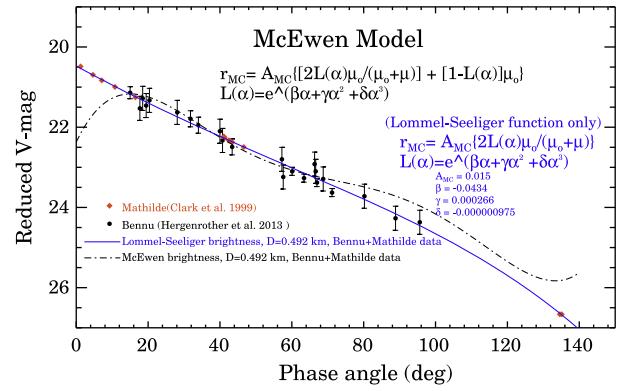


Fig. 5. The reduced V magnitude of Benu as a function of phase angle predicted by the McEwen model (blue solid line) and the Lommel-Seeliger model (black dash-dots) are shown compared with the ground-based measurements. $L(a)$ is a partition parameter between the Lommel-Seeliger and Lambert functions. The McEwen model works reasonably well between 20° and 70° . When the Lambert term was removed from the lunar-Lambert model, the new model becomes equivalent to the Lommel-Seeliger model described in this paper and works well in fitting Benu ground-based observations. (For interpretation of the references to color in this figure legend, the reader is referred to the web version of this article.)

that describes the intrinsic properties of the surface materials, including composition, grain size, roughness, and porosity. In Eq. (20), $B_0(a)$ is independent of the incidence (i) and emission (e) angles. Using the following phase function $f(a) = e^{ba+ca^2+da^3}$, we found that the McEwen’s model does not fit Benu ground-based observations. Even though, this model works reasonably well at phase angles from 20° to 70° (Fig. 5). However, when the Lambert term was removed from the lunar-Lambert model, the new model becomes equivalent to the Lommel-Seeliger model described in this paper and works well in fitting Benu ground-based observations. These results suggest that the lunar-Lambert model of McEwen (1986, 1991) may not be suitable for Benu.

4.3. Application to OSIRIS-REx mission data processing

The Minnaert, Lommel-Seeliger, and ROLO models are useful for predicting flux and brightness quantities for Benu at a wide range of viewing geometries, which provide important information to engineers designing OSIRIS-REx instruments (Fig. 6).

Spectral mapping of the surface of Benu is performed using the four spectral filters (470, 550, 700, 853 nm) of OSIRIS-REx Mapping

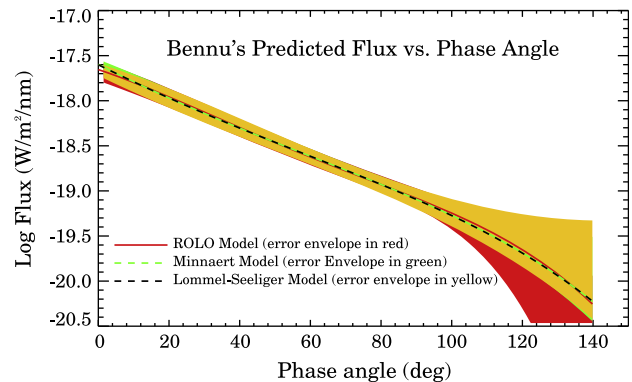


Fig. 6. The logarithm of flux in $W/m^2/nm$ as a function of phase angle predicted by the ROLO model (red solid line with an error envelope in red), the Minnaert model (green dashes with an error envelope in green), and the Lommel-Seeliger model (black dashes with an error envelope in yellow). Note that the Minnaert model and the Lommel-Seeliger model have the same fit. (For interpretation of the references to color in this figure legend, the reader is referred to the web version of this article.)

Camera (MapCam) based on the Eight Color Asteroid Survey (ECAS) b, v, w and x filters (Tedesco et al., 1982). All of these data will be photometrically modeled and photometrically corrected with the best fit model, as described in this work. The wavelength range of MapCam includes broad spectral features that are observed on a wide variety of carbonaceous asteroids, and allow direct comparison with ground-based observations using the same ECAS filters. MapCam images will provide geologic context at the meter-scale for the high-spectral-resolution data acquired by OVIRS and OSIRIS-REX Thermal Emission Spectrometer (OTES) (Hamilton and Christensen, 2014) and guide sample site selection.

OSIRIS-REX will perform extensive global mapping of the surface spectral characteristics with comprehensive spectral coverage (0.4–50 μm) and global spatial resolution of <50 m/pixel using OVIRS and OTES instruments. Combined data from these two instruments allow the identification and quantification of all compounds having spectral absorptions >5% in this wavelength range. This data set will provide information on the distribution and composition of minerals and organic material across the surface of Bennu. It will allow the first analysis of surface processing of carbonaceous material and will guide sample site selection, ensuring maximum science return from the samples. In addition, any spectral diversity observed across the surface after photometrically correcting the data will be used to understand how material is being displaced, providing important clues to the geological and geophysical evolution of Bennu.

When the mission is complete, Bennu will have been observed across a very wide range of solar phase angles and electromagnetic wavelengths. We will have global disk-resolved observations from 5° ($\pm 5^\circ$) up to 90° ($\pm 5^\circ$), and more extreme observations (higher and lower phase angles) of selected regions on the surface. It will be very exciting to synthesize all of these data for a more comprehensive understanding of this very dark asteroid. It will be very exciting to synthesize all of these data for a more comprehensive understanding of this very dark asteroid.

5. Conclusions

In this paper, we showed that three empirical models (Minnaert, Lommel-Seeliger, and ROLO) work equally well in fitting the best ground-based photometric phase curve data of the OSIRIS-REX target Asteroid (101955) Bennu. These models capture the light scattering properties of the surface and subsequently allow us to compute the geometric albedo, phase integral, and spherical Bond albedo for Bennu, which has a low reflectance and geometric albedo, where multiple scattering is not significant. However, these models cannot be used to infer physical properties of Bennu's surface material. We selected these three models because they are simple empirical models with uncoupled and uniquely determined parameter values that can be used to photometrically correct mission data quickly after data acquisition. Other semi-physical models such as the Hapke model, where many assumptions and approximations are necessary, and the McEwen model, are not fully constrained by the available ground-based data of Bennu.

RADFs will be used to model the disk-resolved brightness when the OSIRIS-REX spacecraft arrives at Asteroid Bennu. Our geometric albedo values of $0.047^{+0.012}_{-0.014}$, $0.047^{+0.005}_{-0.014}$, and $0.048^{+0.012}_{-0.022}$ for the Minnaert model, Lommel-Seeliger, and ROLO models respectively are consistent with albedo of 0.045 ± 0.015 computed by Hergenrother et al. (2013, 2014) and Emery et al. (2014). Additionally, our spherical albedo values of $0.010^{+0.005}_{-0.004}$, $0.015^{+0.003}_{-0.001}$, and $0.015^{+0.007}_{-0.005}$ for the Minnaert model, Lommel-Seeliger, and ROLO models respectively are consistent with the Bond albedo of 0.017 ± 0.002 calculated by Emery et al. (2014).

Acknowledgments

We thank Lucille Le Corre and a second reviewer for their thorough comments. We are grateful for thoughtful discussions by Peter Smith, Ellyne Kinney Spano, John Ivens, Bashar Rizk, Brent Bos, Megan Kelleher, Linda Crandall, Yoni Saltzman, Josh Emery, and Chris Voth. The OSIRIS-REX mission is funded by the NASA New Frontiers Program.

References

- Buratti, J. et al., 2012. A wavelength-dependent visible and infrared spectrophotometric function for the Moon based on ROLO data. *J. Geophys. Res.* 116, E00G03.
- Buratti, B., Veverka, J., 1983. Voyager photometry of Europa. *Icarus* 55, 93–110.
- Campins, H., Rieke, G.H., Lebofsky, M.J., 1985. Absolute calibration of photometry at 1 through 5 μm . *Astron. J.* 90, 896–899.
- Chandrasekhar, S., 1960. *Radiative Transfer*. Dover, New York.
- Chesley, S.R. et al., 2013. Orbit and bulk density of the OSIRIS-REX target Asteroid (101955) Bennu. *Icarus* 235, 5–22.
- Clark, B.E. et al., 1999. NEAR photometry of Asteroid 253 Mathilde. *Icarus* 140, 53–65.
- Clark, B.E. et al., 2011. Asteroid (101955) 1999 RQ36: Spectroscopy from 0.4 to 2.4 μm and meteorite analogs. *Icarus* 216, 462–475.
- Emery, J.P. et al., 2014. Thermal infrared observations and thermophysical characterization of OSIRIS-REX target Asteroid (101955) Bennu. *Icarus* 234, 17–35.
- Hamilton, V., Christensen, P., 2014. The OSIRIS-REX Thermal Emission Spectrometer (OTES). *EGU*, vol. 16, p. 4687-1.
- Hapke, B., 2012. *Theory of Reflectance and Emittance Spectroscopy*. Cambridge University Press.
- Hergenrother, C.W. et al., 2013. Lightcurve, color and phase function photometry of the OSIRIS-REX target Asteroid (101955) Bennu. *Icarus* 226, 663–670.
- Hergenrother, C.W. et al., 2014. The design reference asteroid for the OSIRIS-REX Mission Target (101955) Bennu. <<http://arxiv.org/abs/1409.4704>>.
- Lambert, J.H., 1759. *Le perspective affranchie de l'embaras du Plan geometral*. Zurich: Heidegger, 1759; VIII, 192p.: 6 tavv.f.t.; in 8.; DCC.16.29.
- Lauretta, D.S. et al., 2015. The OSIRIS-REX target Asteroid 101955 Bennu: Constraints on its physical, geological, and dynamical nature from astronomical observations. *Meteorit. Planet. Sci.* <http://dx.doi.org/10.1111/maps.12353>
- Lester, T.P., McCall, M.L., Tatum, J.B., 1979. *Theory of planetary photometry*. *J. R. Astron. Soc. Can.* 73, 233–257.
- Li, J.Y. et al., 2009. Photometric analysis of the nucleus of Comet 81P/Wild 2 from Stardust images. *Icarus* 204, 209–226.
- Li, J.Y. et al., 2015. Asteroid photometry. In: *Asteroids IV*. Univ. of Arizona Press, Tucson, submitted for publication.
- Markwardt, C.B., 2008. Non-linear least squares fitting in IDL with MPFIT. In: Bohlender, D., Dowler, P., Durand, D. (Eds.), *Proc. Astronomical Data Analysis Software and Systems XVIII*, Quebec, Canada. ASP Conference Series, vol. 411. Astronomical Society of the Pacific, San Francisco, pp. 251–254. ISBN: 978-1-58381-702-5.
- McEwen, A.S., 1986. Exogenic and endogenic albedo and color patterns on Europa. *J. Geophys. Res. Solid Earth* 91 (B8), 8077–8097.
- McEwen, A.S., 1991. Photometric functions for photoclinometry and other applications. *Icarus* 92, 298–311.
- Minnaert, M., 1941. The reciprocity principle in lunar photometry. *Astrophys. J.* 93, 403–410.
- Nolan et al., 2013. Shape model and surface properties of the OSIRIS-REX target Asteroid (101955) Bennu from radar and lightcurve observations. *Icarus* 226, 629–640.
- Pravec, Harris, 2007. Binary asteroid population 1. Angular momentum content. *Icarus* 190, 250–259.
- Reuter, D., Simon-Miller, A., 2012. The OVIRS visible/IR spectrometer on the OSIRIS-REX Mission. *International Workshop on Instrumentation for Planetary Missions* (abstract #1074).
- Rieke, G.H. et al., 2008. Absolute physical calibration in the infrared. *Astron. J.* 135, 2245–2263.
- Seeliger, H., 1884. Zur photometrie des saturnringes. *Astron. Nachr.* 109, 305–314. <http://dx.doi.org/10.1002/asna.18841092002>.
- Shepard, M.K., Helfenstein, P., 2007. A test of the Hapke photometric model. *J. Geophys. Res. - Planets* 112, 03001.
- Simonelli, D. et al., 1998. Photometric properties of Phobos surface materials from Viking images. *Icarus* 131, 52–77.
- Simon-Miller, A., Reuter, D., 2013. OSIRIS-REX OVIRS: A scalable visible to near-IR spectrometer for planetary study. *Lunar Planet. Sci.* 44. Abstract #1100.
- Tedesco, E.F., Tholen, D.J., Zellner, B., 1982. The Eight-Color Asteroid Survey Standard stars. *Astron. J.* 87, 1585–1592.
- Thuillier, G. et al., 2003. The solar spectral irradiance from 200 to 2400 nm as measured by the SOLSPEC spectrometer from the Atlas and Eureka missions. *Solar Phys.* 214 (1), 1–22.

BIDIRECTIONAL REFLECTANCE AND ALBEDO QUANTITIES

Introduction: Most reflectance and albedo quantities are unitless quantities and are frequently misused or confused. Here, we review these quantities and summarize how viewing conditions vary for each quantity, relevant to OSIRIS-REx. Caution: our target asteroid is very dark, and multiple scattering is assumed to be relatively unimportant, but this assumption may not hold for brighter asteroids.

I. Bidirectional Reflectance Quantities

1. Radiance Factor (RADF)

Hapke:

*Radiance Factor (RADF) is the **ratio** of the bidirectional reflectance of a surface **to** that of a perfectly diffuse surface illuminated at $i = 0$ (the Sun!), rather than at the same angle of illumination.*

(Hapke 1993)

$$RADF(i, e, \alpha) = \pi r(i, e, \alpha),$$

where

$$r(i, e, \alpha) = \frac{\bar{\omega}_o}{4\pi} \frac{\mu_o}{\mu_o + \mu} \{ [1 + B(\alpha)] p(\alpha) + H(\mu_o)H(\mu) - 1 \} S(i, e, \alpha),$$

(The factor of π here is from the normalization and integration of the $p(\alpha)$).

(Hapke 1993 eq. 8.89)

$\mu_o = \cos(i)$, $\mu = \cos(e)$, i is the incidence angle (degrees), e is the emission angle (degrees), $\bar{\omega}_o$ is the average particle single scattering albedo, $1 + B(\alpha)$ is the opposition effect, $p(\alpha)$ is the average particle single-scattering phase function, $(H(\mu_o)H(\mu) - 1)$ describes the isotropic multiple scattering of light, and $S(i, e, \alpha)$ is the macroscopic roughness.

Thus,

$$\begin{aligned} RADF(i, e, \alpha) &= \frac{\bar{\omega}_o}{4} \frac{\mu_o}{\mu_o + \mu} \{ [1 + B(\alpha)] p(\alpha) + H(\mu_o)H(\mu) - 1 \} S(i, e, \alpha) \\ &= \pi r(i, e, \alpha) = [I/\mathcal{F}](i, e, \alpha), \end{aligned}$$

I is the radiance and has units of $\text{W}/\text{m}^2/\text{nm}/\text{steradian}$. $J = \pi\mathcal{F}$ is the collimated light (irradiance) and has units of $\text{W}/\text{m}^2/\text{nm}$. Strictly speaking I/\mathcal{F} is a dimensionless quantity (\mathcal{F} has units of $\text{W}/\text{m}^2/\text{nm}/\text{steradian}$ and π here has units of steradian).

(Hapke 1993)

(RADF $[I/\mathcal{F}]$ is what is measured by the spacecraft)

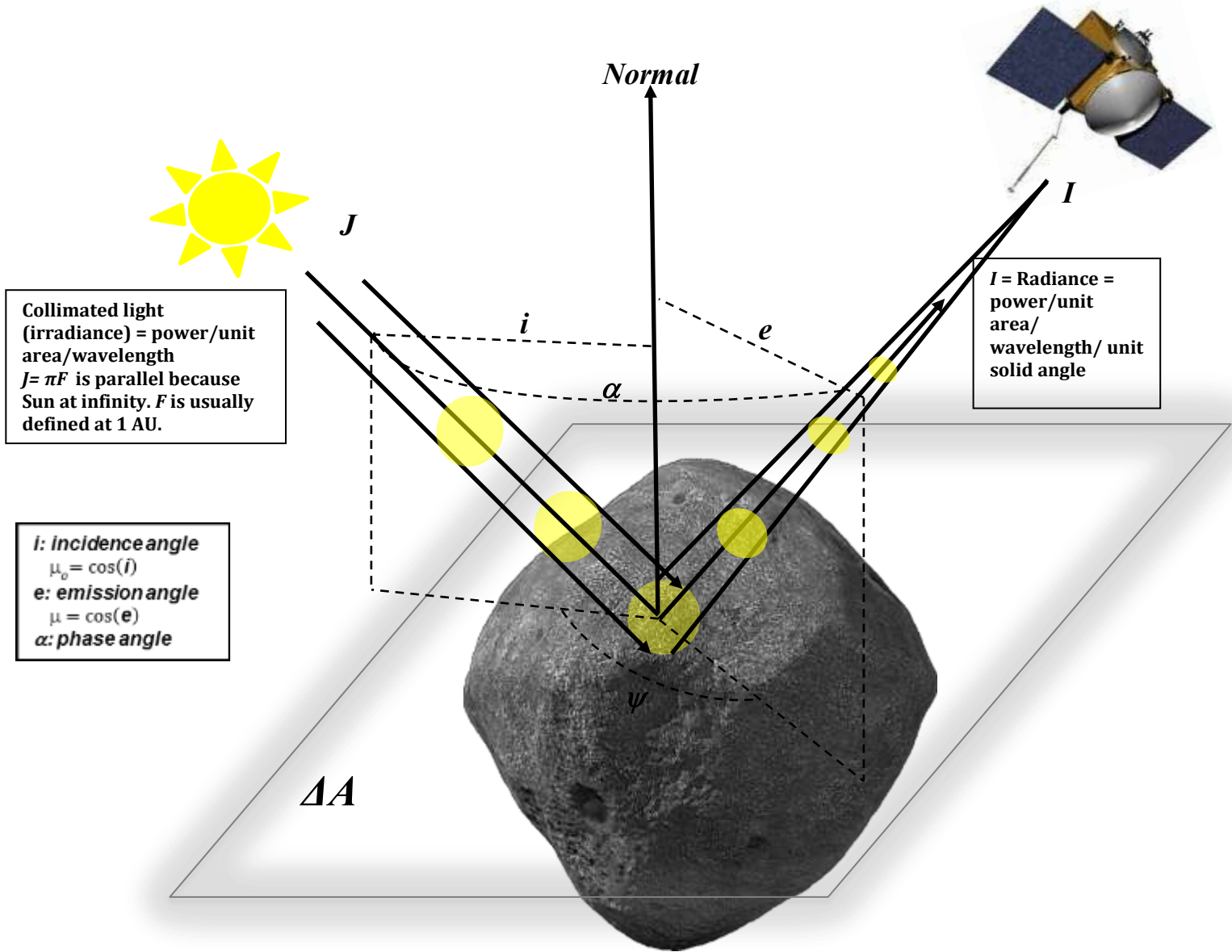


Figure 1. Schematic diagram of bidirectional reflectance from a surface element ΔA , showing the various angles. The plane containing J and I is the scattering plane. If the scattering plane also contains N , it is called the principal plane. ψ is the azimuthal angle between the planes of incidence and emission [$\cos(\alpha) = \cos(i)\cos(e) + \sin(i)\sin(e)\cos(\psi)$.]
 [Adopted from Hapke (1993)]

Lambert Model:

$$RADF(i, e, \alpha) = A_L \mu_o = [I/\mathcal{F}](i, e, \alpha),$$

where A_L is the Lambert albedo.

(Lambert 1759)

The Lambert model is a disk function that accounts only for limb darkening. However, A_L could be a function of phase angle (α).

Lambert Model with the Phase Function:

$$RADF(i, e, \alpha) = A_L f(\alpha) \mu_o = [I/\mathcal{F}](i, e, \alpha),$$

where $f(\alpha) = 10^{-\frac{(\beta\alpha + \gamma\alpha^2 + \delta\alpha^3)}{2.5}}$ is a 3rd order polynomial phase function.

(d'Aubigny 2011)

This Lambert model accounts for limb darkening *and* the surface phase function.

Minnaert Model Disk Function:

$$RADF(i, e, \alpha) = \pi A_M \mu_o^k \mu^{k-1} = [I/\mathcal{F}](i, e, \alpha),$$

(Minnaert 1941)

where A_M and k are model parameters that characterize the Minnaert albedo and limb-darkening behavior of the surface, respectively.

The Minnaert disk function accounts only for limb darkening. However, both πA_M and k could be functions of phase angle (α).

Minnaert Model with the Phase Function:

$$RADF(i, e, \alpha) = \pi A_M f(\alpha) \mu_o^{k(\alpha)} \mu^{k(\alpha)-1} = [I/\mathcal{F}](i, e, \alpha),$$

where $f(\alpha) = 10^{-\beta\alpha/2.5}$, β is the phase slope, and $k(\alpha) = k_o + b\alpha$ characterizes the limb-darkening behavior of the surface and b captures the linear relationship between k and phase angle (α). k_o is the value of k at zero degrees phase angle.

(Li et al. 2009)

Or

$$f(\alpha) = 10^{-\frac{(\beta\alpha + \gamma\alpha^2 + \delta\alpha^3)}{2.5}}$$

(d'Aubigny 2011)

This Minnaert model includes the effects of limb darkening *and* the surface phase function.

Note: when $i = 0$ $\mu_o \rightarrow 1$ and $e = 0$ $\mu \rightarrow 1$, $RADF(0,0,0) = \pi A_M f(\alpha)$, which is consistent with normal reflectance when $f(\alpha)$ is normalized to 1 at $\alpha = 0$.

Lommel-Seeliger Disk Function:

$$RADF(i, e, \alpha) = \frac{\bar{\omega}_o}{4} \frac{\mu_o}{\mu_o + \mu} = [I/\mathcal{F}](i, e, \alpha),$$

(Seeliger 1884)

where $\bar{\omega}_o$ is the average particle single scattering albedo and $f(\alpha)$ is an arbitrary function that describes the variation in surface reflectance with phase angle.

The Lommel-Seeliger disk function accounts only for limb darkening. However, $\bar{\omega}_o$ could be a function of phase angle(α).

Lommel-Seeliger Model with the Phase Function:

$$RADF(i, e, \alpha) = \frac{\bar{\omega}_o}{4} \frac{\mu_o}{\mu_o + \mu} f(\alpha) = [I/\mathcal{F}](i, e, \alpha),$$

(Helfenstein and Veverka 1989)

where $f(\alpha)$ is an arbitrary function that describes the variation in surface reflectance with phase angle (α), and $A_{LS} = \frac{\bar{\omega}_o}{4\pi}$ is Lommel-Seeliger albedo.

$$f(\alpha) = e^{\beta\alpha + \gamma\alpha^2 + \delta\alpha^3}$$

This Lommel-Seeliger/Veverka model includes the effects of limb darkening *and* the surface phase function.

ROLO Model:

$$RADF(i, e, \alpha) = \underbrace{\frac{\mu_o}{\mu_o + \mu}}_{\text{Describes limb darkening}} f(\alpha) = [I/\mathcal{F}](i, e, \alpha),$$

Describes limb darkening ←

Where $f(\alpha) = \underbrace{C_0 e^{-C_1 \alpha}}_{\text{Describes opposition surge}} + \underbrace{A_0 + A_1 \alpha + A_2 \alpha^2 + A_3 \alpha^3 + A_4 \alpha^4}_{\text{4th order polynomial that describes phase function}}.$ (Buratti et al. 2011)

Describes opposition surge ←

4th order polynomial that describes phase function →

The ROLO model includes the effects of limb darkening *and* the surface phase function.

(These are the RADFs we will use to model Bennu's surface)

2. Reflectance Factor (REFF)

*Reflectance Factor (or reflectance coefficient) (REFF) is the **ratio** of the reflectance of the surface **to** that of a perfectly diffuse (Lambert) surface under the same conditions of illumination.*

(Hapke 1993)

$$REFF(i, e, \alpha) = \frac{r(i, e, \alpha)}{\frac{\mu_o}{\pi}} = \frac{\pi r(i, e, \alpha)}{\mu_o},$$

Thus

$$REFF(i, e, \alpha) = \frac{\bar{\omega}_o}{4} \frac{1}{\mu_o + \mu} \{ [1 + B(\alpha)] p(\alpha) + H(\mu_o)H(\mu) - 1 \} S(i, e, \alpha) = \frac{[I/\mathcal{F}](i, e, \alpha)}{\mu_o}$$

(This reflectance quantity is what is measured in the laboratory. For OVIRS spectral indices, the OVIRS data will be in these units.)

$$REFF(i=0, e=0, \alpha=0) = \frac{I/\mathcal{F}(i=0, e=0, \alpha=0)}{\mu_o} = \text{Normal Reflectance.}$$

(This is the most reasonable quantity to use when mapping the “albedo” of the surface.)

3. Hapke Bidirectional Reflectance Distribution Function (BRDF)

*Bidirectional Reflectance Distribution Function (BRDF) is the **ratio** of the radiance scattered by a surface into a given direction **to** the collimated power incident on a unit area of the surface.*

(Hapke 1993)

$$BRDF(i, e, \alpha) = \frac{Jr(i, e, \alpha)}{J\mu_o} = \frac{r(i, e, \alpha)}{\mu_o},$$

$J\mu_o$ is the incident radiant power per unit area of surface and $Jr(i, e, \alpha)$ is the scattered radiance.

Thus

$$\begin{aligned} BRDF(i, e, \alpha) &= \frac{\bar{\omega}_o}{4\pi} \frac{1}{\mu_o + \mu} \{ [1 + B(\alpha)] p(\alpha) + H(\mu_o)H(\mu) - 1 \} S(i, e, \alpha) \\ &= [I/(\mu_o \pi \mathcal{F})](i, e, \alpha). \end{aligned}$$

(Functions of this form are requested by OSIRIS Instrument Teams to be used to predict Bennu’s brightness. See conclusion Table 2 showing relationship between RADF and BRDF.)

II. Albedo Quantities

1. Lambertian Albedo

Lambertian albedo (A_L) is the **ratio** of the total power scattered per unit area of a Lambert surface to the incident power per unit area.

(Hapke 1993)

$$A_L = \frac{P_L}{J\mu_o},$$

$P_L = \int_{2\pi} I(i, e, \alpha) \mu d\alpha = \int_{e=0}^{\pi/2} \int_{\alpha=0}^{2\pi} JK_L \cos i \cos e \sin e de d\alpha = \pi JK_L \mu_o$ is the total power scattered per unit area of Lambert surface into all directions of the upper hemisphere.

Where $K_L = r_L(i, e, \alpha)/\mu_o$ is a constant (*Lambert's law*). When K_L is constant then we have a Lambertian surface.

Thus the *Lambert reflectance* is $\pi r_L(i, e, \alpha) = A_L \mu_o = RADF(i, e, \alpha) = [I/\mathcal{F}](i, e, \alpha)$.

Therefore

$$A_L = [I/(\mu_o \mathcal{F})](i, e, \alpha).$$

2. Geometric Albedo

Physical albedo (a.k.a, Geometric albedo) (A_{geo}) is the **ratio** of the brightness of a body at zero phase angle $\alpha = 0$ to the brightness of a perfect *Lambert disk* of the same radius and at the same distance as the body, but illuminated and observed perpendicularly.

(Hapke 1993)

$$A_{geo} = \int_{2\pi} r(e, e, 0) \mu d\Omega,$$

where $d\Omega = 2\pi \sin(e) de = -2\pi d\mu$.

Geometric Albedo is usually presented at one wavelength, the V passband, or 0.55 μm .

2.1 Lommel_Seeliger

$$A_{geo} = \frac{A_{LS}}{2} \pi f(0) \int_0^{\pi/2} \cos(e) \sin(e) de = \frac{A_{LS}}{2} \pi f(0)$$

2.2 ROLO

$$A_{geo} = f(0) \int_0^{\pi/2} \cos(e) \sin(e) de = \frac{f(0)}{2}$$

2.3 Minnaert:

$$A_{geo} = 2\pi A_M f(0) \int_0^{\pi/2} [\cos(e)]^{2k_o} \sin(e) de = A_M \frac{2\pi}{2k+1} f(0)$$

k_o is the value of $k(\alpha)$ at zero degrees phase angle.

3. Normal Albedo

The *normal albedo* A_n is the ratio of the brightness of a surface observed at zero phase angle from an arbitrary direction to the brightness of a perfectly diffuse surface located at the same position, but illuminated and observed perpendicularly.



$$A_n = \frac{[Jr(e,e,0)]}{[\frac{J}{\pi}]} = \pi r(e, e, 0)$$

4. Spherical Bond Albedo

Spherical bond albedo (a.k.a., *Bond albedo*) (A_{sph}) is the total fraction of incident irradiance at one wavelength (usually 0.55 μm) scattered by the body into all directions.

(Hapke 1993)



$$A_{sph} = \frac{1}{\pi} \int_{2\pi} \int_{2\pi} r(i, e, \alpha) \mu d\Omega_i d\Omega_e,$$

where $d\Omega_i = \sin(i) di d\psi$ and $d\Omega_e = \sin(e) de d\psi$ with ψ is the azimuth.

The *spherical bond* albedo can also be expressed as $q A_{geo}$, where q is the phase integral, defined as:

$$q = 2 \int_0^\pi \Phi(\alpha) \sin(\alpha) d\alpha$$

where $\Phi(\alpha) \equiv \frac{F(\alpha)}{F(0^\circ)}$ is the disk-integrated brightness at phase angle α , assuming a spherical body

(Buratti and Veverka 1983). $F(\alpha)$ is the phase dependence of the disk-integrated flux defined as:

$$F(\alpha) = \frac{R^2}{r^2} \int_{\alpha-\frac{\pi}{2}}^{\frac{\pi}{2}} \int_{\alpha-\frac{\pi}{2}}^{\frac{\pi}{2}} \frac{I}{F}(i, e, \alpha) \cos(w) \cos^2(\psi) dw d\psi,$$

where w = photometric longitude, ψ = photometric latitude, R = radius of the satellite, and r = observer-satellite distance.

(This is the albedo quantity shown in Table 1 that requires observations covering phase angles from $0^\circ \rightarrow 180^\circ$.)

4. Bolometric Bond Albedo

Bolometric bond albedo (A_{bolo}) is the average of the spherical *Bond albedo* $A_{sph}(\lambda)$ weighted by spectral irradiance of the Sun $J_S(\lambda)$. This integrates *Spherical albedo* over all λ .

$$A_{bolo} = \frac{\int_0^{\infty} A_{sph}(\lambda) J_S(\lambda) d\lambda}{\int_0^{\infty} J_S(\lambda) d\lambda},$$

where $J_S(\lambda)$ is the solar flux spectrum (λ).

(The OSIRIS-REx Science Team has adopted the solar flux model of Reike et al. 2008)

(This is the quantity required for Yarkovsky and thermal inertia measurements for OSIRIS-REx)

III. Examples of Reflectance and Albedo Quantities:

Table 1a. Comparison of reflectance and albedo quantities for different asteroids:

	Ceres ⁰	Ida ¹	Eros ²	Eros ³	Dactyl ¹	Gaspra ¹	Mathilde ⁴	Vesta ⁵	Bennu ^{6,7}	Phobos ⁸	Deimos ⁸
Geometric Albedo	0.088	0.206	0.290	0.23	0.198	0.23	0.047	0.38±0.01	0.045	0.071	0.068
Spherical Bond Albedo	0.020	0.081	0.12	0.093	0.073	0.12	--	0.20±0.02	0.016	0.021	0.027
Normal Reflectance	--	0.207	--	--	0.198	0.23	0.047	--	--	0.071	0.068

⁰Li et al. (2006). ¹Helfenstein et al. 1994, ²Domingue et al. 2002, ³Li et al. 2004, ⁴Clark et al. 1999, ⁵Li et al. 2013, ⁶Hergenrother et al. 2013. ⁷Emery et al. (2014). The geometric albedo and normal reflectance values are for 0.55 μ m. Note that Helfenstein and Domingue do not seem to agree on the meaning of Bond albedo terms. ⁸Simonelli et al. (1998) and Thomas et al. (1996).

Table 1b. Comparison of reflectance and albedo quantities for different comets:

	9P/Tempel 1 ¹	19P/Borrelly ²	81P/Wild 2 ³	28P/Neujmin 1 ⁴	2P/Encke ⁵
Geometric Albedo	0.059±0.009	0.080±0.020	0.059	0.026	0.047
Spherical Bond Albedo	0.014±0.002	0.018	0.0093	--	--

¹Li et al. (2013).²Li et al. (2007).³Li et al. (2009).⁴Campins et al. (1987).⁵Fernandez et al. (2000)

IV. Conclusions

- The value of albedo measured with an integrating sphere (in the laboratory) can be comparable to the *spherical bond* albedo of a body covered with the same material (Barucci et al. 2012).
- The *bolometric bond* albedo is *not* equal to the *spherical bond* albedo. The bolometric albedo is the average of the spectral bond albedo weighted by spectral irradiance of the Sun.
- It is generally assumed that the *spherical bond* albedo in the V passband (~0.55 μm) is a good representation of the *bolometric bond* albedo. This is because (a) most of the Sun's energy is in the visible and (b) most spectra of Solar System bodies do not change drastically over the UV/Vis (Emery, personal communication).
- For disk-resolved observations and Lommel-Seeliger surfaces, the value of $I/(\mu_o\mathcal{F})$ is close to the value of the *geometric* albedo at wavelength λ when observed at a phase angle $\alpha = 0$. $I/\mathcal{F} = 1$ is for a flat *Lambertian* surface when viewed at normal incidence.
- For disk-integrated observations and Lommel-Seeliger surfaces, the *geometric* albedo, which is similar to the *normal* albedo, is a measure of a surface's brightness relative to a perfectly scattering Lambertian disk.
- The Lambert and Minnaert functions are disk functions with no dependence on phase angle and account only for limb darkening. However, the Hapke, Minnaert, the Lommel-Seeliger/Veverka, and ROLO functions include surface phase functions and limb darkening.
- For Bennu and other dark objects, the normal reflectance value is close to $(1/\pi)$ times the geometric albedo value for Lommel-Seeliger surfaces. The normal reflectance is the most reasonable quantity to use when mapping the "albedo" of the surface.
- Lester et al. (1979), who called the normal albedo (p_n), found that the geometric albedo (p) is equivalent to the normal albedo (p_n) for Lommel-Seeliger surfaces.
- **Table 2.** In this table we show various models converted from RADF to BRDF by division of $\pi\mu_o$. Note that in our equations, I/\mathcal{F} is unitless, where I = measured radiance from the surface in $\text{W}/\text{m}^2/\text{sr}/\text{nm}$ and $J = \pi\mathcal{F}$ = solar irradiance (flux) in $\text{W}/\text{m}^2/\text{nm}$. π has units of steradian and \mathcal{F} units of $\text{W}/\text{m}^2/\text{nm}/\text{steradian}$.

	RADF	BRDF
	$[I/\mathcal{F}](i, e, \alpha) =$	$\frac{[I/\mathcal{F}](i, e, \alpha)}{\pi\mu_o} =$
<i>Lambert Model</i>	$A_L f(\alpha)\mu_o$	$\frac{A_L f(\alpha)}{\pi}$
<i>Minnaert Model</i>	$\pi A_M f(\alpha)\mu_o^{k(\alpha)} \mu^{k(\alpha)-1}$	$A_M f(\alpha)\mu_o^{k(\alpha)-1} \mu^{k(\alpha)-1}$
<i>Lommel Seeliger Model</i>	$\frac{\bar{\omega}_o}{4} \frac{\mu_o}{\mu_o + \mu} f(\alpha)$	$\frac{\bar{\omega}_o}{4\pi} \frac{1}{\mu_o + \mu} f(\alpha)$
<i>ROLO Model</i>	$\frac{\mu_o}{\mu_o + \mu} f(\alpha)$	$\frac{1}{\pi} \frac{1}{\mu_o + \mu} f(\alpha)$

References

- Barucci, M.A., Belskayaa, I.N., Fornasier, S., Fulchignoni, M., Clark, B.C., Coradini, C., Capaccioni, F., Dotto, E., Birlan, M., Leyrat, C., Sierks, H., Thomas, N., Vincenti, J.B. 2012. Overview of Lutetia's surface composition. *Planetary & Space Science* 66, 23-30.
- Blackburn, D.G., Buratti, B.J., Ulrich, R., Mosher, J.A. 2012. Solar phase curves and phase integrals for the leading and trailing hemispheres of Iapetus from the Cassini Visual Infrared Mapping Spectrometer. *Icarus* 209, 738-744.
- Buratti, J., Hicks, M.D., Nettles, J., Staid, M., Pieteres, C.M., Sunshine, J., Boardman, J., and Stone, T.C. 2012. A wavelength-dependent visible and infrared spectrophotometric function for the Moon based on ROLO data. *JGR* 116, E00G03.
- Campins, H., A'Hearn, M.F., McFadden, L.A., 1987. The bare nucleus of Comet Neujmin 1. *Astrophys. J.* 316, 847-857.
- Clark, B.E., Veverka, J., Helfenstein, P., Thomas, P. C.; Bell, J. F., Harch, A., Robinson, M. S., Murchie, S. L., McFadden, L. A., Chapman, C. R. 1999. NEAR Photometry of Asteroid 253 Mathilde. *Icarus* 140, 53-65.
- Clark, B.E., Binzel, R. P., Howell, E.S., Cloutis, E.A., Ockert-Bell, M., Christensen, P., Barucci, M.A., DeMeo, F., Lauretta, D.S.; Connolly, H., Soderberg, A., Hergenrother, C., Lim, L.; Emery, J., Mueller, M. 2011. Asteroid (101955) 1999 RQ36: Spectroscopy from 0.4 to 2.4 μm and meteorite analogs. *Icarus* 216, 462-475.
- Domingue, D.L., Robinson, M., Carcich, B., Joseph, J., Thomas, P, Clark, B.E. 2002. Disk-integrated Photometry of 433 Eros. *Icarus* 155, 205-219.
- Drouet Aubigny, C. 2011. RQ36 Photometric Models and Their Implications for OCAMS. Draft V6.
- Fernández, Y.R., Lisse, C.M., Käufel, H.U., Peschke, Sibylle B., Weaver, H.A., A'Hearn, M.F., Lamy, P.L., Livengood, T.A., Kostiuk, T., 2000. Physical properties of the nucleus of Comet 2P/Encke. *Icarus* 147, 145-160.
- Hapke, B. 1993. *Theory of Reflectance and Emittance Spectroscopy*. Cambridge University Press.

- Hergenrother et al. 2013. The Design Reference Asteroid Document. OSIRIS-REx Mission.
- Helfenstein, P., Veverka, J., Thomas, P.C., Simonelli, D.P., Lee, P., Klaasen, K., Johnson, T.V., Breneman, H., Head, J.W., Murchie, S., Fanale, F., Robinson, M., Clark, B., Granahan, J., Garbeil, H., McEwen, A.S., Kirk, R.L., Davies, M., Neukum, G., Mottola, S., Wagner, R., Belton, M., Chapman, C., and Plicher, C. 1994. Galileo Photometry of Asteroid 951 Gaspra. *Icarus* 107, 37-60.
- Helfenstein and Veverka. 1989. Physical characterization of asteroid surfaces from photometric analysis. In *Asteroids II*. Univ. of Arizona Press, Tucson.
- Lambert, J.H., 1759. *L perspective affranchie de l'embaras du Plan geometral*. Zurich: Heidegger, 1759; VIII, 192 p. : 6 tavv.f.t. ; in 8.; DCC.16.29.
- Li, J.Y., A'Hearn, M.F., and McFadden, L.A. 2004. Photometric analysis of Eros from NEAR data. *Icarus* 172, 415-431.
- Li, J.Y., McFadden, L.A., Parker, J.W., Young, E.F., Thomas, P.C., Russell, C.T., Sykes, M.V., Stern, S.A., 2006. Photometric analysis of 1 Ceres and surface mapping from HST observations. *Icarus* 182, 143-160.
- Li, J.Y., A'Hearn, M.F., McFadden, L.A., Belton, M.J.S. 2007. *Icarus* 188, 195-211. *Icarus* 188 (2007) 195-211.
- Li, J.Y., A'Hearn, M.F., Farnham, T.L., McFadden, L.A., 2009. Photometric analysis of the nucleus of Comet 81P/Wild 2 from Stardust images. *Icarus* 204, 209-226.
- Li, J.Y., A'Hearn, M.F., Belton, M.J.S., Farnham, T., L., Klaasen, K.P., Sunshine, J.M., Thomas, P.C., Veverka, J. 2013. Photometry of the nucleus of Comet 9P/Tempel 1 from Stardust-NExT flyby and the implications. *Icarus* 222, 467-476.
- Minnaert, M. 1941. The Reciprocity Principle in Lunar Photometry. *Astrophys. J.* 93, 403-410.
- Rieke, G.H., Blaylock, M., Decin, L., Engelbracht, C., Ogle, P., Avrett, E., Carpenter, J., Cutri, R.M., Armus, L., Gordon, K., Gray, R.O., Hinz, J., Su, K., and Willmer, C.N.A. Absolute Physical Calibration in the Infrared. *The Astronomical Journal.* 135:2245-2263.
- Seeliger, H. 1884. Zur Photometrie des Saturnringses, *Astron. Nachr.*, 109, 305-314, doi:10.1002/asna.18841092002
- Simonelli, D., M. Wisz, A. Switala, D. Adinolfi, J. Veverka, P. C. Thomas, and P. Helfenstein 1998. Photometric properties of Phobos surface materials from Viking images. *Icarus* **131**, 52-77.
- Thomas, P. C., J. Veverka, J. F. Bell III, B. E. Clark, B. Carcich, J. Joseph, M. Robinson, L. A. McFadden, M. C. Malin, C. R. Chapman, W. Merline, and S. L. Murchie 1999. Mathilde: Size, shape and geology. *Icarus* **140**, 17-27.
- Takir, D., Clark, B.C., D'Aubigny, C.D., Hergenrother, C.W., Li, J.Y., Lauretta, D.S., and Binzel, R.P. Photometric models of disk-integrated observations of the OSIRIS-REx target Asteroid (101955) Bennu. Volume 252, Pages 393-399.



Photometric Modeling Workflow

